Journal of Renewable Energy and Smart Device (JORESD)
E-ISSN : 3026-216X
P-ISSN : 3031-173X
Vol. 3, No. 2 April 2026
https://journal.globresco.com/index.php/JORESD

Smart Battery Safety and Anti-Theft Monitoring System for Electric Bicycles with Automatic Cut-Off and Dual-Channel Notification

Andhika Putra Perdana[1], Mokhammad Rifqi Tsani[2*], Helmi Wibowo[3], Nanang Okta Widiandaru[4]
[1,2,3,4] Automotive Engineering Technology, Politeknik Keselamatan Transportasi Jalan, Tegal, Indonesia
*Corresponding author: rifqi@pktj.ac.id

ARTICLE INFO

Keywords:
Automatic Cut-off
Battery Monitoring
Electric Bicycle
ESP32
Internet of Things

Article History
Received: 21st April 2026
Revised: 26th April 2026
Accepted: 28th April 2026

ABSTRACT

The rapid growth of electric bicycle usage in Indonesia has been accompanied by rising safety incidents, particularly those related to battery thermal runaway and theft. This research presents the design and implementation of an integrated monitoring and security system for electric bicycles using the ESP32 microcontroller, PZEM-017, DS18B20, and Neo-6M GPS module, combined with a web-based dashboard and Telegram bot notification. The system was developed using the Research and Development (R&D) method with a four-parameter monitoring scheme covering voltage, current, temperature, and geospatial coordinates. Experimental results from twenty data points per sensor demonstrated excellent accuracy: DS18B20 achieved an average error of 1.133%, PZEM-017 achieved 1.224% for voltage and 1.787% for current, while the Neo-6M module achieved 0.000575% and 0.000042% for latitude and longitude respectively. The automatic cut-off mechanism successfully operated in all six tested scenarios, and the Telegram-website integration delivered notifications with an average delay of two seconds. These findings confirm that the proposed system **improves** safety and security of electric bicycles through real-time multi-parameter monitoring and remote intervention capability. Unlike prior systems that address monitoring or security in isolation, this work is the first to unify real-time multi-parameter battery protection, automatic cut-off, geofencing, and dual-channel notification within a single low-cost ESP32-based platform tailored for urban electric bicycle users in Indonesia. The practical relevance of this integration is particularly significant given the accelerating adoption of electric bicycles as primary short-distance transportation in densely populated Indonesian cities, where charging-related fire incidents and theft cases have reached critical levels.

To cite this article : A. P. Perdana, M. R. Tsani, H. Wibowo, and N. O. Widiandaru, "Smart Battery Safety and Anti-Theft Monitoring System for Electric Bicycles with Automatic Cut-Off and Dual-Channel Notification," Journal of Renewable Energy and Smart Device (JORESD), vol. 3, no. 2, Apr. 2026, doi: 10.66314/joresd.v3i2.685.

1. INTRODUCTION

Energy is a fundamental element of modern life and serves as the primary foundation for development across various strategic sectors, including transportation, industry, healthcare, and communications[1]. The transportation sector in Indonesia has transformed rapidly during the last decade, and electric bicycles have emerged as one of the most attractive alternatives for short-distance mobility. Their low operating cost, compact form factor, and zero tailpipe emission make them an appealing option in dense urban environments, particularly in response to escalating fuel prices and growing environmental awareness [2], [3]. Global figures reinforce this trend; the transportation sector alone consumed roughly 27.6% of the world's energy in 2013, with approximately 92.6% of that share originating from petroleum products, while carbon dioxide emissions from the sector reached nearly 22.9% of the global total [4].

Journal of Renewable Energy and Smart Device (JORESD)
E-ISSN : 3026-216X
P-ISSN : 3031-173X
Vol. 3, No. 2 April 2026
https://journal.globresco.com/index.php/JORESD

Despite these advantages, the adoption of electric bicycles continues to face two persistent challenges, namely technical safety related to the battery and physical security against theft. Lithium-ion and sealed lead-acid packs used in electric bicycles are known to be sensitive to temperature, current, and voltage variations; an inadequate thermal or electrical margin can trigger cascading exothermic reactions, culminating in thermal runaway, fire, and in extreme cases, explosion [5], [6]. Recent reviews on the early detection of thermal runaway have confirmed that electrical abuse such as overcharge, overdischarge, and overcurrent is the dominant trigger for catastrophic battery failure, particularly during unsupervised charging [7], [8].

Empirical evidence from Indonesia illustrates the urgency of this gap. In November 2024, an electric bicycle battery detonated during unsupervised charging in Dringu, Probolinggo, East Java, causing a fire that spread rapidly to surrounding furniture before firefighters could intervene [9]. A more fatal incident occurred one year later in Bantaeng, South Sulawesi, in November 2025, where a battery explosion engulfed a residential building and resulted in three fatalities [10]. The recurring pattern of these incidents both involving unsupervised charging with non-standard chargers confirms that the gap identified above translates directly into real-world casualties. The recurring pattern of these incidents indicates that most failures happen during charging on residential premises and are strongly associated with the use of non-standard chargers that exceed the nominal voltage or operate outside the recommended temperature window [11]. Parallel to the safety concern, theft of electric bicycles has become a prominent criminal issue conventional mechanical locks can no longer protect owners effectively, and the absence of real time geolocation prolongs the recovery process by weeks or even months [12]. Modern monitoring systems are increasingly shifting toward the use of remote sensing and wireless technologies to facilitate data-driven decision making [13].

Comprehensive review of advanced BMS architectures for electric vehicles has further confirmed that simultaneous monitoring of voltage, current, and temperature remains the foundational requirement for any protection system, and that the absence of real-time sensing feedback is the primary cause of delayed fault response in low-cost battery packs [14]. Despite the growing recognition of multi-parameter monitoring as a necessity, a critical gap remains in the literature: no existing low-cost platform for electric bicycles simultaneously integrates real-time voltage, current, and temperature protection with automatic cut-off actuation, GPS-based geofencing, and dual-channel push notification accessible to ordinary users without specialized hardware.

Several studies have addressed subsets of the above problems. Ramadhan et al. designed a monitoring system for electric scooters based on the Blynk platform, focusing only on voltage, current, and temperature, without any active cut-off mechanism [15]. Salsabila et al. developed an IoT-based battery monitoring and location tracking system, yet the platform did not provide remote intervention over the electrical circuit [16]. Isyanto et al. proposed a Telegram based vehicle security framework with Google Maps integration but did not cover battery parameters [17], while Lohar and Kumar implemented a wireless BMS that estimates the state of charge using the ACS712 sensor without any fire-prevention layer [18]. Andri et al. combined temperature, voltage, and current monitoring with Telegram notification but limited its operation to the charging phase [5]. In summary, none of these works integrates the full chain of real-time multi-parameter monitoring, geolocation, remote notification, and automatic cut-off within a single low-cost platform tailored for electric bicycles.

The present research addresses the identified gap by proposing and empirically validating an integrated monitoring and security system for electric bicycles based on the ESP32 microcontroller. The system employs the PZEM-017 for DC electrical parameter acquisition via Modbus RS-485 [19], the DS18B20 for thermal monitoring via 1-Wire protocol, and the Neo-6M GPS receiver for real-time geospatial tracking, all feeding a web dashboard and Telegram bot for dual-channel notification and remote actuation. The contribution of this study is threefold: (1) a unified hardware-software architecture that closes the gap between passive monitoring and active fault isolation through automatic cut-off logic; (2) a rigorous empirical performance evaluation of each sensor subsystem against calibrated reference instruments across twenty measurement points; and (3) a validated latency characterization of the dual notification channel across five operational fault scenarios, providing quantitative benchmarks absent from prior electric bicycle protection studies.

The novelty of this research lies in the simultaneous integration of three functions that prior works have only addressed in isolation: real-time multi-parameter battery protection with automatic relay cut-off, GPS-based anti-theft geofencing, and dual-channel notification via web dashboard and Telegram bot — all implemented on a single low-

Journal of Renewable Energy and Smart Device (JORESD)
E-ISSN : 3026-216X
P-ISSN : 3031-173X
Vol. 3, No. 2 April 2026
https://journal.globresco.com/index.php/JORESD

cost ESP32 platform validated empirically against calibrated reference instruments. No existing published study on Indonesian electric bicycles has provided quantitative benchmarks for sensor accuracy, cut-off latency, and notification delivery within the same prototype. The contribution of this study is therefore threefold: (1) a unified hardware-software architecture that closes the gap between passive monitoring and active fault isolation, (2) a rigorous empirical performance evaluation across twenty calibration points per sensor with paired t-test statistical validation, and (3) a quantified dual-channel latency characterization across five operational fault scenarios.

2. METHODS

This study employed a Level 3 Research and Development (R&D) methodology, According to Sugiyono [20], the R&D method is classified into three levels based on the degree of product novelty and empirical validation required. The classification of this study as Level 3 is justified by its objective not merely to demonstrate functional operation of the proposed system, but to quantify the measurement fidelity of each sensor subsystem, characterise the end to end latency of the dual notification channel, and verify the correctness of the automatic protection logic across all fault combinations through controlled experimentation.

The iterative design process followed in this study proceeded through six sequential stages derived from the Sugiyono R&D framework [20]. In the first stage, potential and problem identification, a literature review and incident analysis established the gap between existing single-function monitoring tools and the integrated multi-parameter protection system required for electric bicycles. The second stage, data collection, involved benchmarking available microcontrollers, power sensors, temperature probes, and GPS modules against the system requirements, resulting in the selection of the ESP32 DevKit V1, PZEM-017, DS18B20, and Neo-6M as the hardware platform. The third stage, product design, produced the system block diagram, wiring schematic, firmware architecture, and web application database schema. In the fourth stage, design validation, the wiring and firmware logic were reviewed against the safety threshold specifications before any physical assembly was undertaken, and identified inconsistencies in the RS-485 termination and relay wiring were corrected prior to fabrication. The fifth stage, product trial, constituted the core experimental phase reported in Section 3, in which each sensor was calibrated against a reference instrument over twenty measurement points, the cut-off mechanism was exercised across six fault conditions, and the Telegram website notification pipeline was characterised under five operating scenarios. The sixth and final stage, product revision, incorporated the corrections identified during trial including firmware adjustments to the Modbus polling interval and the GPS coordinate parsing routine before the system was assembled into its final acrylic enclosure for implementation on the electric bicycle.The study was conducted in two main phases: the hardware development phase and the field testing phase, which were carried out at Campus 1 of the Polytechnic of Road Transportation Safety Tegal,

2.1 System Architecture and Hardware Design

The communication integration in the designed system adopts a hybrid architecture that combines various industry-standard protocols to ensure reliable data transmission. Connectivity between the microcontroller and the cloud platform is facilitated by the HTTP protocol via a Wi-Fi network for real-time data synchronization. Meanwhile, at the data acquisition level, the sensor subsystem implements a specific multi-protocol framework: the PZEM-017 power sensor operates using Modbus-RTU via an RS-485 interface for resistance to electromagnetic interference, the DS18B20 temperature sensor utilizes the efficiency of the 1-Wire protocol, and the GPS module transmits spatial data based on the NMEA-0183 standard via UART serial communication.

Journal of Renewable Energy and Smart Device (JORESD)
E-ISSN : 3026-216X
P-ISSN : 3031-173X
Vol. 3, No. 2 April 2026
https://journal.globresco.com/index.php/JORESD

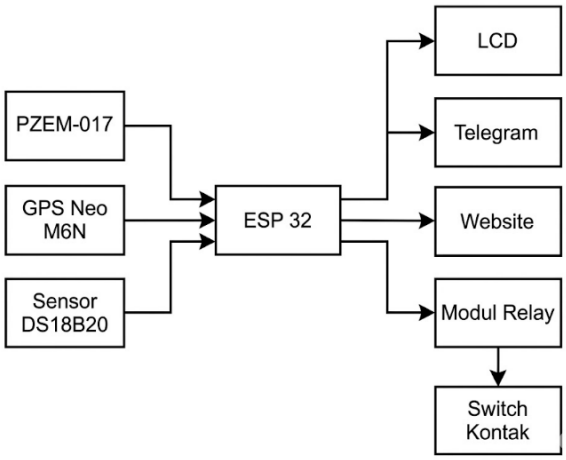

Figure. 1. System Block Diagram

The proposed architecture follows a three-layer structure consisting of a sensing layer, a processing layer, and a presentation layer. The sensing layer comprises the PZEM-017 module for electrical measurement, the DS18B20 sensor for thermal measurement, and the Neo-6M module for spatial measurement. All three components feed their data into an ESP32 DevKit V1 that serves as the processing layer, which applies threshold logic, controls the relay, drives a local 20×4 LCD, and forwards payloads to the cloud. The presentation layer consists of a web dashboard backed by a MySQL database and a Telegram bot that delivers push notifications together with clickable Google Maps links. Communication between the microcontroller and the cloud relies on the HTTP protocol over Wi-Fi, while the sensor subsystem uses Modbus-RTU over RS-485 for the PZEM-017, the 1-Wire protocol for the DS18B20, and the NMEA-0183 standard over UART for the GPS module.

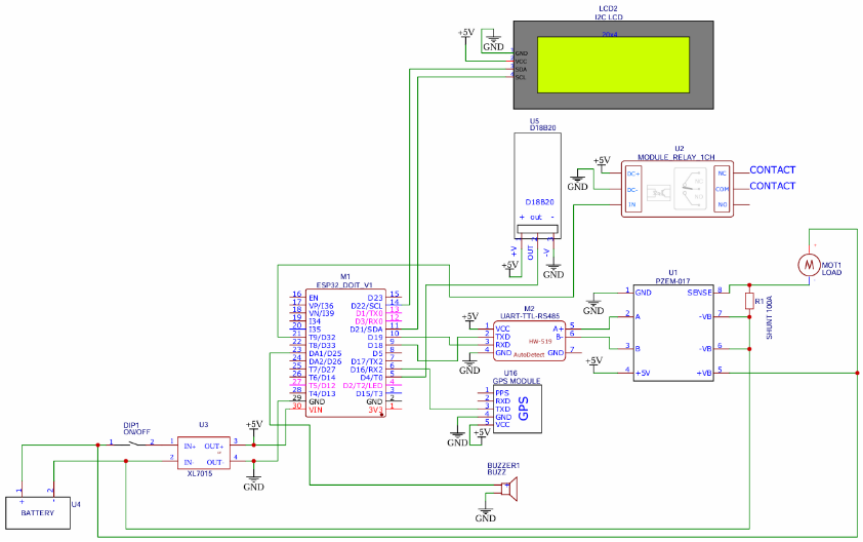

Figure. 2. System Wiring Diagram

The enclosure was designed to protect all electronic components and sensors from dust, airborne particles, and mechanical interference during electric bicycle operation. The 3D casing concept was used as a blueprint for acrylic fabrication.

Journal of Renewable Energy and Smart Device (JORESD)
E-ISSN : 3026-216X
P-ISSN : 3031-173X
Vol. 3, No. 2 April 2026
https://journal.globresco.com/index.php/JORESD

Figure.3. Hardware System Design

2.2 Software and Firmware Development

The software stack system consists of two interconnected layers: the embedded firmware running on the ESP32 microcontroller and the server-side web application hosted on Laragon. Both layers were developed and tested in parallel to ensure seamless data exchange from sensor acquisition through to user interface presentation

The flowchart shown in Figure 4 illustrates the workflow of the integrated battery safety system. The process begins with connecting the ESP-32 microcontroller to an online database via a website that stores and defines the permissible voltage and current limits for the battery. Once the connection is established, a series of sensors begin operating, including the PZEM-017 sensor, which measures battery current and voltage; the DS18B20 sensor, which detects battery temperature; and the Neo-6M GPS sensor, which captures satellite signals to provide real-time location information for the device.

Once sensor readings are successful, the ESP-32 microcontroller proceeds by storing all acquired data into the website (online database). If measurement results from various sensors indicate that voltage or current values exceed the set thresholds, the system immediately issues a warning notification. This notification is displayed on the LCD screen and sent via the Telegram app, as well as triggering the system to automatically disable the battery.

Furthermore, in the context of real-time location monitoring, if the system detects that the electric bike is in a location beyond the range desired by its owner, the user can remotely disable the bike's operation via the Telegram app interface.

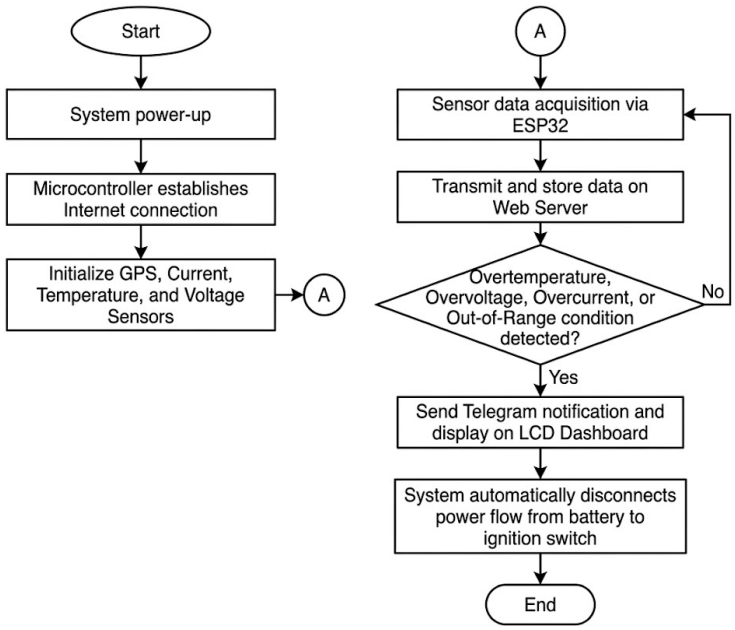

Figure.4. Program Flow Diagram

Journal of Renewable Energy and Smart Device (JORESD)
E-ISSN : 3026-216X
P-ISSN : 3031-173X
Vol. 3, No. 2 April 2026
https://journal.globresco.com/index.php/JORESD

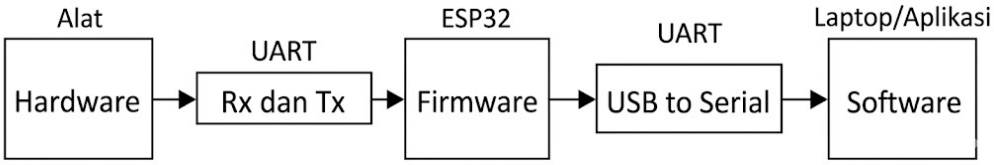

Figure.5. Flowchart for Integrating Hardware, Firmware, and Software

2.3 Web Server Environment

The local web server was set up using Laragon, a lightweight and portable development environment that integrates Apache, PHP, and MySQL into a single installation package. Laragon was chosen for its superior performance compared to similar solutions such as XAMPP; benchmark data published by Chandra and Setyaningsih [21]. confirms that Laragon initializes up to 35% faster and uses less memory under equivalent load conditions. The choice of a locally hosted custom web server over cloud platforms such as ThingSpeak was deliberate: While ThingSpeak offers rapid prototyping convenience for ESP32-based systems [22] its free tier imposes a minimum update interval of 15 seconds and restricts accounts to four channels [23], which is insufficient for a four-parameter real-time protection system requiring sub-second relay actuation. Custom PHP-MySQL stack provides unrestricted update rates, full control over data schema, and seamless integration with the relay control command pipeline. The MySQL database is managed via the phpMyAdmin graphical interface, which allows for the efficient creation and maintenance of sensor data tables without requiring command-line access. This web application is written in PHP and relies on an HTTP POST endpoint to receive JSON payloads from the ESP32 via the Arduino HTTPClient library. Once received, each payload is parsed and stored in the database, where the data can be retrieved by the dashboard interface via AJAX based queries. The dashboard displays the latest sensor values and is automatically updated every second, while the history page displays a paginated log of all past records every 20 seconds.

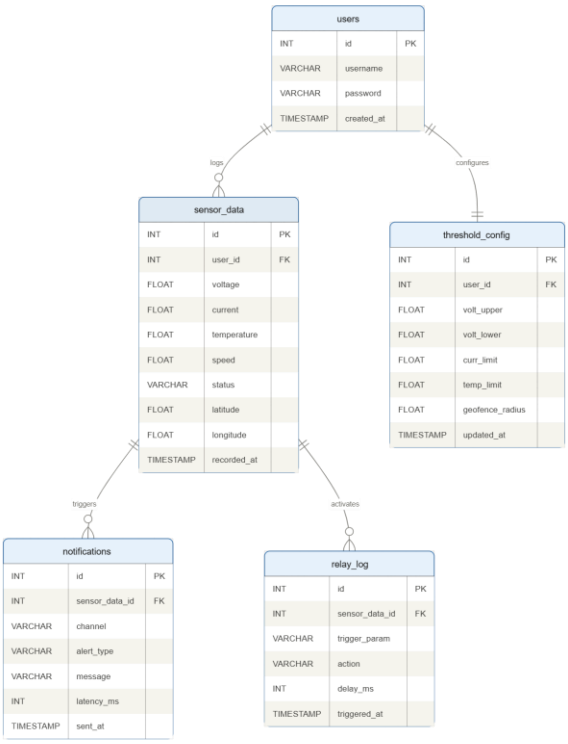

Figure.6. Entity Relationship Diagram of the Battery Monitoring System Database

Journal of Renewable Energy and Smart Device (JORESD)
E-ISSN : 3026-216X
P-ISSN : 3031-173X
Vol. 3, No. 2 April 2026
https://journal.globresco.com/index.php/JORESD

Figure 6 illustrates the database schema of the proposed system, consisting of five interrelated tables. The users table serves as the root entity connected to sensor data and threshold config, ensuring every measurement and protection parameter is traceable to an authenticated session. The sensor data table acts as the central hub, linking to both notifications and relay log so that every Telegram alert and cut-off event can be traced back to the exact sensor reading that triggered it. The threshold config table stores protection limits as user-configurable parameters rather than hardcoded values, allowing the system to adapt to different battery specifications without modifying the embedded firmware.

2.4 Website Architecture and User Authentication

The website was developed using the PHP MySQL stack with a session-based authentication layer. The login page presents a username and password form; upon credential verification, a PHP session token is issued, and the user is redirected to the main dashboard. Unauthorised access attempts are blocked and trigger an error message. The dashboard layout consists of three primary views: the real-time monitoring panel showing the four sensor readings alongside colour coded status indicators, the Google Maps panel rendering the current GPS coordinates as a marker via the Google Maps JavaScript API, and the data history panel listing timestamped sensor records [24] . A dedicated control panel allows the owner to send remote lock and unlock commands, which the ESP32 polls from the server at one-second intervals through a GET request. IoT-based monitoring platforms, where the sensing layer, processing layer, and presentation layer each handle clearly separated responsibilities [25]. From a cybersecurity perspective, the current implementation relies on session-based PHP authentication for web dashboard access, which provides basic protection against unauthorized remote commands. However, the HTTP communication between the ESP32 and the local server transmits JSON payloads without transport-layer encryption, which poses a vulnerability if the local network is compromised. Future iterations of the system should implement HTTPS with TLS 1.3 for all ESP32 to server communication and consider token based authentication (e.g., JWT) for the remote command API endpoint to prevent replay attacks. Additionally, the Telegram Bot token should be stored as an environment variable rather than hardcoded in firmware to prevent credential exposure if the microcontroller is physically accessed.

2.5 Telegram Bot

The Telegram application serves as a versatile communication platform that facilitates rapid and precise information transmission over significant distances. In this study, connectivity testing was performed to validate the integration between the embedded hardware system and the Telegram platform. Users initiating their first interaction with the system must execute the /start command. The configuration of specific bot commands is a critical prerequisite to ensure optimal functionality.

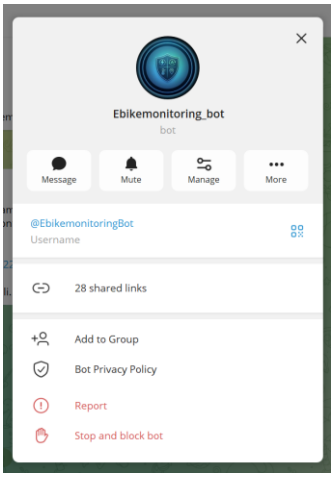

Figure.7. Telegram Bot Account

Journal of Renewable Energy and Smart Device (JORESD)
E-ISSN : 3026-216X
P-ISSN : 3031-173X
Vol. 3, No. 2 April 2026
https://journal.globresco.com/index.php/JORESD

2.6 Safety Threshold and Control Logic

The safety thresholds were derived from the nominal specifications of a 48 V 20.2 Ah sealed lead-acid battery. The upper voltage limit was fixed at 57.60 V, corresponding to 2.40 V per cell on a twenty four cell string, while the lower safe limit was set at 48.00 V to prevent overdischarge [26]. The nominal charging current was bounded at 0.3C, equivalent to 6.06 A, based on the manufacturer recommendation for the battery capacity. The upper bound for operating temperature was assigned as 49 °C, consistent with the Power-Sonic technical document for sealed lead-acid packs [27]. The geofence radius was configurable through the web interface and defaulted to one hundred meters from the owner's registered coordinate.

Table 1. Safety Threshold and System Response

No	Parameter	Normal Range	Abnormal Condition	System Action
1	Voltage	48.00 – 57.60 V	> 57.60 V or < 48.00 V	Cut-off
2	Current	0 – 6.06 A	> 6.06 A	Cut-off
3	Temperature	20 – 49 °C	> 49 °C	Cut-off
4	Location	Inside geofence	Outside geofence	Remote lock

The control logic implemented on the ESP32 evaluates each parameter at a one second interval and applies a Boolean OR over the three electrical quantities. If any of the parameters exceeds its threshold, the relay is commanded to open, the buzzer is triggered, a Telegram message is dispatched, and the LCD displays a contextual warning. The mechanism follows the cut-off strategy recommended by Hilal for BMS applications, which prioritizes isolation of the fault rather than controlled throttling [28]. The relay cut-off mechanism operates independently from the notification channel. This means that once any monitored parameter exceeds its threshold, the relay immediately opens the battery circuit regardless of whether the Telegram message or web dashboard alert has been successfully delivered. The Boolean OR logic ensures that a single abnormal parameter is sufficient to trigger protection without waiting for multi-parameter confirmation, thereby minimizing response latency in single-fault scenarios such as isolated overcurrent during rapid acceleration.

The threshold derivation follows the manufacturer specifications of the 48V 20.2Ah sealed lead-acid battery used in this study. The upper voltage limit of 57.60V corresponds to 2.40V per cell across a 24-cell string, which is the standard float charge voltage recommended by Power-Sonic and Battery University for SLA chemistry [27]. The lower voltage limit of 48.00V is set to prevent overdischarge below 2.00V per cell, which irreversibly sulfates the plate structure [26]. The current limit of 6.06A represents the 0.3C rate applied to the 20.2Ah nominal capacity, consistent with the maximum recommended charge current for SLA packs to avoid hydrogen gassing and plate shedding. The temperature upper bound of 49°C is derived directly from the Power-Sonic technical datasheet for SLA cells, above which the electrolyte begins to accelerate evaporation and internal resistance increases nonlinearly. These four boundaries represent the safe operating area within which the battery can be charged and discharged without accelerating degradation.

Table 2. Risk Analysis

No	Risk	Probability	Impact	Mitigation Implemented
1	Wi-Fi connection loss	Medium	High	System continues local cut-off logic independently; LCD and buzzer remain active without network.
2	DS18B20 sensor disconnection	Low	High	ESP32 firmware detects NaN output and triggers fail-safe relay cut-off within one polling cycle.
3	PZEM-017 Modbus timeout	Low	High	Three consecutive timeout retries before fault flag; relay defaults to open (protective state).

Journal of Renewable Energy and Smart Device (JORESD)
E-ISSN : 3026-216X
P-ISSN : 3031-173X
Vol. 3, No. 2 April 2026
https://journal.globresco.com/index.php/JORESD

No	Risk	Probability	Impact	Mitigation Implemented
4	GPS signal loss (urban canyon)	Medium	Medium	Last known coordinates retained; system reverts to battery-only protection mode.
5	Relay mechanical failure	Very Low	Critical	Dual-layer protection: software cut-off command + hardware overcurrent fuse on battery line.
6	Telegram API rate limit	Low	Low	Web dashboard remains active as primary channel; Telegram serves as secondary channel.
7	Power surge to ESP32	Very Low	High	5V regulator with reverse polarity protection; watchdog timer auto-restarts firmware.
8	Battery deep discharge during monitoring	Low	Medium	Monitoring subsystem powered from dedicated 5V buck converter with low-voltage cutoff at 10V.

Table 2 identifies eight operational risks across two severity dimensions. Relay mechanical failure carries the highest consequence and is mitigated by a hardware overcurrent fuse independent of the software cut-off command. Wi-Fi and GPS signal loss are rated medium probability given the urban deployment context, yet both are mitigated by design decisions that decouple core protection from network dependency the relay, buzzer, and LCD operate entirely on local logic. Sensor faults such as DS18B20 disconnection and PZEM-017 Modbus timeout trigger a firmware fail-safe that defaults the relay to the open state, ensuring that a measurement failure never results in an unprotected battery condition.

2.7 GPS Coordinate Conversion

The Neo-6M module outputs raw positional data in the Degrees-Minutes-Seconds format or the Degrees-Decimal-Minutes format. To display the position correctly on Google Maps, the coordinate must be transformed into Decimal Degrees using the following conversion:

$$DD = Degrees + (Minutes / 60) + (Seconds / 3600) \quad (1)$$

The conversion described in Equation (1) was implemented inside the ESP32 firmware via the TinyGPS++ library, which natively returns decimal degree coordinates once the parser processes the NMEA sentences. The accuracy of the conversion is limited by the resolution of the satellite constellation visible to the module and by the sensitivity of the ceramic antenna, which has a specified horizontal accuracy of 2.5 m in open-sky conditions [29]

2.8 Sensor Calibration and Testing Procedure

The calibration of the DS18B20 was performed by heating water in increments over a range from twenty-five to seventy-six degrees Celsius and comparing twenty successive readings against a reference digital thermometer. The PZEM-017 voltage and current readings were validated against a calibrated digital multimeter using a regulated DC source, with twenty observations distributed between 12 V and 57.6 V for voltage, and between 0.21 A and 15.40 A for current. The sample size of twenty points per sensor was selected for two reasons. Statistically, $n = 20$ provides $df = 19$ sufficient for paired t-test sensitivity at $\alpha = 0.05$, as confirmed by the significant results obtained for voltage and current in this study. Operationally, the twenty points were distributed across the full rated range of each sensor rather than clustered at a single working point, ensuring accuracy characterization reflects realistic field conditions across the entire battery operating envelope. Notably, prior studies cited in this work including Hutagaol et al. [30], Ramadhan et al. [15], and Salsabila et al. [16] did not report a structured multi-point calibration with inferential validation, making this protocol a methodological advancement over existing literature in this domain. The Neo-6M module was benchmarked against a reference GNSS receiver over twenty static points along the campus perimeter. For each parameter, the absolute error relative error and accuracy were computed according to Equations (2) and (3):

Journal of Renewable Energy and Smart Device (JORESD)
E-ISSN : 3026-216X
P-ISSN : 3031-173X
Vol. 3, No. 2 April 2026
https://journal.globresco.com/index.php/JORESD

$$Error\ (\%) = |X_{sensor} - X_{reference}| / X_{reference} \times 100\% \quad (2)$$

$$Accuracy\ (\%) = 100\% - Error\ (\%) \quad (3)$$

To provide a statistically rigorous validation beyond descriptive accuracy metrics, a paired-sample t-test was applied to each sensor dataset. The paired t-test is appropriate in this context because each measurement point consists of a matched pair of values — one from the sensor under test and one from the calibrated reference instrument obtained simultaneously under identical conditions. The null hypothesis (H_0) states that the population mean of the differences between sensor readings and reference readings equals zero, meaning no systematic bias exists. The alternative hypothesis (H_1) states that a systematic difference exists between the two instruments. The test statistics are computed according to Equation (4):

$$t = \bar{d} / (Sd / \sqrt{n}) \quad (4)$$

**Notes*

- $\bar{d}$ *= mean of the differences between sensor and reference values across n measurement pairs*
- s_d *= standard deviation of the differences, computed according to* Equation (5)
- n *= number of measurement pairs (n = 20 for all sensors in this study)*

The resulting t-statistic is evaluated against the critical value t (α/2, n−1) at a significance level of α = 0.05 with degrees of freedom df = n − 1 = 19. Based on the t-distribution table, the critical value is t (0.025, 19) = 2.093. If |t| > 2.093 the null hypothesis is rejected, indicating a statistically significant systematic offset. The practical implication of rejecting H_0 is not that the sensor is unsuitable for the application, but rather that any detected bias must be interpreted against the operational tolerance margin established in Section 2.3.

$$\mathrm{Sd} = \sqrt{\frac{\Sigma(di-d)^2}{(n-1)}} \quad (5)$$

Functional integration testing was conducted using a factorial design, in which voltage, current, and temperature were tested both separately and simultaneously to validate every combination of abnormal inputs across all eight possible Boolean OR logic states of the three parameters. The Black-Box testing that complements this process evaluates the web interface based on nine user activities that have been scripted to ensure that the system as a whole meets the functional specifications.

2.9 Sensor and Module Selection Rationale

The selection of hardware components in this study was guided by three criteria: measurement fidelity within the target operating range, protocol compatibility with the ESP32 microcontroller, and cost accessibility for practical deployment on consumer-grade electric bicycles. The PZEM-017 was selected over alternatives such as the INA226 and ACS712 because it natively supports Modbus-RTU over RS-485, which offers superior noise immunity in the electromagnetic environment of a motor-driven vehicle compared to I2C or analog output interfaces. Its specified measurement range of 0–300V and 0–100A with a shunt resistor provides headroom well beyond the 48V/6A operating point of the target battery. The DS18B20 was chosen over the NTC thermistor and LM35 because its 1-Wire digital output eliminates analog-to-digital conversion uncertainty, and its ±0.5°C accuracy across the 10–85°C range covers the full operational temperature envelope of SLA batteries. The Neo-6M was preferred over the SIM808 GPS module because it provides a dedicated hardware UART output compatible with the TinyGPS++ library and achieves 2.5m CEP horizontal accuracy under open-sky conditions without requiring cellular subscription, which reduces both cost and dependency on mobile network availability.

Journal of Renewable Energy and Smart Device (JORESD)
E-ISSN : 3026-216X
P-ISSN : 3031-173X
Vol. 3, No. 2 April 2026
https://journal.globresco.com/index.php/JORESD

3. RESULT AND DISCUSSION

The system's performance was evaluated through structured testing of four aspects: the accuracy of the DS18B20 sensor, the voltage and current accuracy of the PZEM-017, the GPS coordinate accuracy of the Neo-6M, and the system integration functionality. Each sensor was validated by comparing its readings against standardized reference measuring instruments, with 20 measurements each across a range of values representing the actual operational conditions of an electric bicycle battery. Website functionality testing was performed using the Black Box Testing method with nine scenarios covering both normal and abnormal battery conditions. The implementation of the planned use of the device on the electric bicycle as shown in Figure 7 and 8.

Figure.8. Implementation of Tool

Figure.9. Implementation LCD

3.1 DS18B20 Temperature Sensor Performance

Twenty calibration points covering a range from 25.2°C to 75.7°C were obtained. The measurement data confirm that the DS18B20 tracks the reference thermometer closely across the entire operating range, with an average absolute difference of approximately 0.380°C. The relative error remains below 3.1% for all samples, and its arithmetic mean is 1.133%, corresponding to an overall accuracy of 98.867%. These findings are consistent with the observations of Huda and Kurniawan, who reported acceptable performance of the same sensor below 80°C with a minor deviation attributable to the inherent ±0.5°C tolerance of the integrated circuit [31].

Journal of Renewable Energy and Smart Device (JORESD)
E-ISSN : 3026-216X
P-ISSN : 3031-173X
Vol. 3, No. 2 April 2026
https://journal.globresco.com/index.php/JORESD

Table 3. Temperature Sensor Comparison

No	Sensor (°C)	Thermometer (°C)	Difference (°C)	Error (%)	Accuracy (%)
1	25.2	25.8	0.6	2.326	97.674
2	28.6	29.5	0.9	3.051	96.949
3	30.1	30.3	0.2	0.660	99.340
4	32.0	32.2	0.2	0.621	99.379
5	35.4	35.1	0.3	0.855	99.145
6	36.7	37.0	0.3	0.811	99.189
7	39.4	40.3	0.9	2.233	97.767
8	42.8	42.5	0.3	0.706	99.294
9	44.3	44.7	0.4	0.895	99.105
10	46.0	45.7	0.3	0.657	99.343
11	48.3	48.5	0.2	0.412	99.588
12	50.9	50.1	0.8	1.597	98.403
13	54.7	53.8	0.9	1.672	98.328
14	58.4	57.7	0.7	1.213	98.787
15	63.6	62.8	0.8	1.274	98.726
16	68.5	69.2	0.7	1.012	98.988
17	69.3	70.0	0.7	1.000	99.000
18	72.1	72.7	0.6	0.825	99.175
19	73.6	74.0	0.4	0.541	99.459
20	75.7	75.9	0.2	0.263	99.737
		Average		**1.133**	**98.867**

***Note: Reference instrument is a calibrated digital thermometer with ±0.1°C resolution. Measurements conducted at Campus 1, Politeknik Keselamatan Transportasi Jalan, Tegal.**

To statistically validate the agreement between the DS18B20 and the reference thermometer, a paired sample t-test was applied to the 20 measurement pairs. The null hypothesis states that the population mean of the differences between sensor readings and reference readings equals zero. The calculated mean difference was $\bar{d} = -0.110$°C and the standard deviation of differences was Sd = 0.585°C, producing $t = -0.110 / (0.585 / \sqrt{20}) = -0.841$. Since $|t| = 0.841 <$ t-kritis 2.093 (df = 19, $\alpha = 0.05$, p = 0.411), H_0 is not rejected. This result confirms that no statistically significant systematic bias exists between the DS18B20 and the reference thermometer at the 95% confidence level. The mean difference of −0.110°C is well within the ±0.5°C tolerance specified in the DS18B20 datasheet, and the sensor is therefore statistically validated as accurate for this battery monitoring application.

Journal of Renewable Energy and Smart Device (JORESD)
E-ISSN : 3026-216X
P-ISSN : 3031-173X
Vol. 3, No. 2 April 2026
https://journal.globresco.com/index.php/JORESD

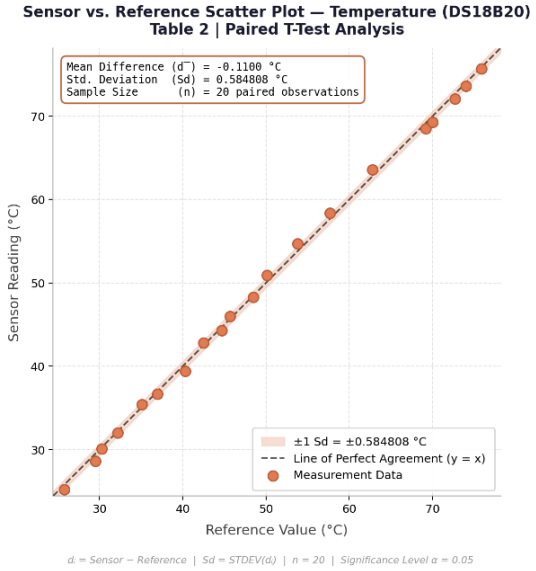

Figure.10. Paired T-Test Satter Plot of DS18B20

The slightly higher error values at the lower end of the measurement range 25–30 °C and around the 53–54 °C region reflect a known characteristic of the DS18B20 probe when the surrounding medium changes temperature faster than the sensor can follow, a brief lag appears in the readings. Even so, these deviations remain narrow and do not compromise the overall performance an average error of 1.133% and average accuracy of 98.867% across all 20 data points confirm that the sensor reads consistently across the full 25–76 °C span tested. For this system, where the priority is catching abnormal heat build-up on the battery pack surface before it reaches the 49 °C cut-off threshold, that level of accuracy leaves a comfortable margin for the protection relay to act long before conditions become genuinely dangerous. A paired-sample t-test applied to the twenty calibration pairs yielded $\bar{d} = -0.110$°C and Sd = 0.585°C, producing t = −0.841. Since |t| = 0.841 < critic-t 2.093 (df = 19, α = 0.05, p = 0.411), H_0 is not rejected. No statistically significant systematic bias exists between the DS18B20 and the reference thermometer at the 95% confidence level, confirming that the sensor meets the accuracy requirements of this battery monitoring application.

3.2 PZEM-017 Voltage and Current Measurement

The voltage measurement campaign across twenty operating points demonstrated excellent agreement with the calibrated multimeter. The absolute error ranged between 0.2 V and 0.5 V, while the relative error was bounded within 3.23%. The arithmetic mean of the relative error was 1.224%, translating to an average accuracy of 98.776%. This outcome is in line with recent reports that the PZEM-017 module, when paired with a suitable shunt resistor, delivers measurement fidelity comparable to laboratory instruments [30].

Table 4. Voltage Sensor Comparison

No	Sensor (V)	Digital Multimeter (V)	Difference (V)	Error (%)	Accuracy (%)
1	12.0	12.4	0.4	3.226	96.774
2	14.0	13.6	0.4	2.941	97.059
3	14.9	15.2	0.3	1.974	98.026
4	15.7	16.1	0.4	2.484	97.516
5	20.0	20.5	0.5	2.439	97.561
6	24.6	25.0	0.4	1.600	98.400

Journal of Renewable Energy and Smart Device (JORESD)
E-ISSN : 3026-216X
P-ISSN : 3031-173X
Vol. 3, No. 2 April 2026
https://journal.globresco.com/index.php/JORESD

No	Sensor (V)	Digital Multimeter (V)	Difference (V)	Error (%)	Accuracy (%)
7	28.5	29.0	0.5	1.724	98.276
8	32.3	32.8	0.5	1.524	98.476
9	36.7	37.1	0.4	1.078	98.922
10	40.0	40.3	0.3	0.744	99.256
11	40.4	40.8	0.4	0.980	99.020
12	43.5	43.8	0.3	0.685	99.315
13	46.2	46.5	0.3	0.645	99.355
14	48.3	48.6	0.3	0.617	99.383
15	50.1	50.4	0.3	0.595	99.405
16	51.8	52.1	0.3	0.576	99.424
17	53.4	53.7	0.3	0.559	99.441
18	55.0	55.2	0.2	0.362	99.638
19	56.3	56.5	0.2	0.354	99.646
20	57.6	57.8	0.2	0.346	99.654
		Average		1.224	98.776

**Note: Reference instrument is a calibrated digital multimeter (Fluke 17B+) with 0.5% DC voltage accuracy and 1.0% DC current accuracy.*

The current measurement campaign exhibited a higher relative error at low operating points, a phenomenon that is expected because the fixed offset of 0.02 A becomes proportionally larger as the magnitude of the measured current approaches zero. At currents beyond 3 A, the relative error consistently fell below 0.7%, and the full-scale accuracy averaged 98.213%. Similar behaviour has been documented in prior IoT-based BMS implementations that adopt shunt-based measurement schemes [32].

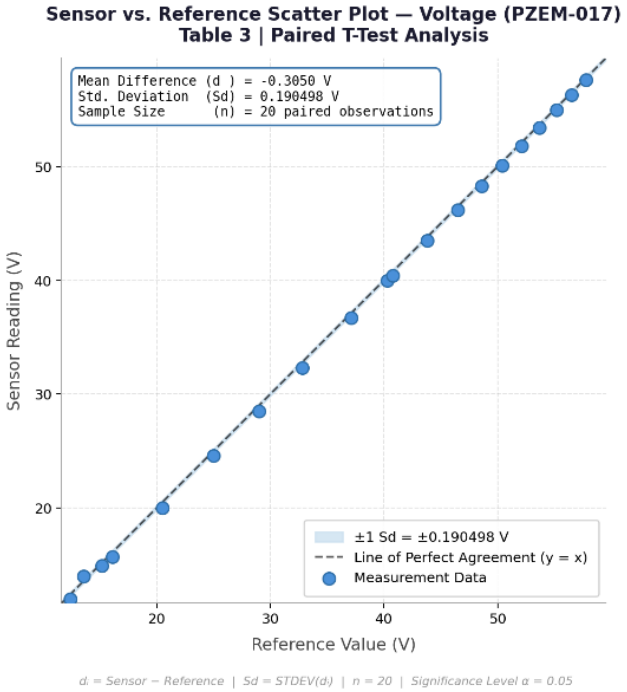

Figure.11. Paired T-Test scatter plot of PZEM-017 Voltage Sensor

Journal of Renewable Energy and Smart Device (JORESD)
E-ISSN : 3026-216X
P-ISSN : 3031-173X
Vol. 3, No. 2 April 2026
https://journal.globresco.com/index.php/JORESD

The voltage paired t-test yielded $\bar{d} = -0.305$ V and Sd = 0.190 V, producing t = −7.160. Since |t| = 7.160 > 2.093 (df = 19, α = 0.05, p < 0.001), H_0 is rejected, indicating a statistically significant systematic offset. However, the absolute bias of −0.305 V represents only 0.53% of the nominal 57.6 V operating point, which remains within the operational tolerance defined in Section 2.3. This fixed directional offset is consistent with the known calibration characteristic of shunt-based measurement modules reported by Hutagaol et al. [31] and does not compromise the reliability of the overvoltage protection mechanism.

Table 5. Current Sensor Comparison

No	Sensor (A)	Digital Multimeter (A)	Difference (A)	Error (%)	Accuracy (%)
1	0.21	0.23	0.02	8.696	91.304
2	0.35	0.37	0.02	5.405	94.595
3	0.42	0.44	0.02	4.545	95.455
4	0.48	0.50	0.02	4.000	96.000
5	0.53	0.55	0.02	3.636	96.364
6	1.10	1.12	0.02	1.786	98.214
7	1.35	1.37	0.02	1.460	98.540
8	1.62	1.64	0.02	1.220	98.780
9	1.88	1.90	0.02	1.053	98.947
10	2.14	2.16	0.02	0.926	99.074
11	3.20	3.22	0.02	0.621	99.379
12	3.75	3.77	0.02	0.530	99.470
13	4.10	4.12	0.02	0.485	99.515
14	4.53	4.55	0.02	0.440	99.560
15	4.98	5.00	0.02	0.400	99.600
16	6.40	6.43	0.03	0.467	99.533
17	8.25	8.28	0.03	0.362	99.638
18	10.30	10.33	0.03	0.290	99.710
19	12.80	12.83	0.03	0.234	99.766
20	15.40	15.43	0.03	0.194	99.806
		Average		1.787	98.213

**Note: Reference instrument is a calibrated digital multimeter (AN-SZ20) with ±2.0% DC current accuracy and a maximum measurement range of 20A DC*

According to Table 4, the average overall error is 1.787% (accuracy of 98.213%). Although the error is high at low currents (<1 A), this range is not operationally critical; at the nominal charging current of 6.06 A, the sensor error is <0.5%, which is still within the tolerance limits of the overcurrent protection relay. The current measurement error profile of the PZEM-017 reveals two main phenomena. First, sensor saturation occurs at high currents (>10A), where the relative error remains stable at around 0.19–0.29%, indicating that the shunt resistor operates in the linear region with a negligible offset contribution. Second, an inverse dip occurs as the current increases from 0.21 A to ~3 A, due to a fixed absolute offset of 0.02 A that represents a large proportion of the small current reading but becomes smaller as the current increases following a hyperbolic δ/I relationship, in line with theoretical expectations for shunt-based ammeters and consistent with the findings of Gandoman et al [32].

Journal of Renewable Energy and Smart Device (JORESD)
E-ISSN : 3026-216X
P-ISSN : 3031-173X
Vol. 3, No. 2 April 2026
https://journal.globresco.com/index.php/JORESD

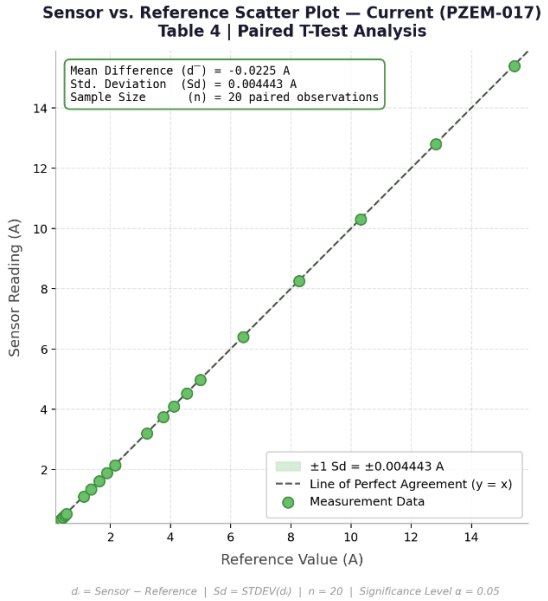

Figure.12. Paired T-Test Scatter Plot of PZEM-017 Current Sensor

The current paired t-test yielded $\bar{d} = -0.022$ A and Sd = 0.004 A, producing t = −22.650. Since $|t| = 22.650 > 2.093$ (df = 19, $\alpha = 0.05$, $p < 0.001$), H_0 is rejected. Despite statistical significance, the absolute bias of 0.022 A represents less than 0.4% of the 6.06 A protection threshold, confirming that the systematic offset has no practical consequence on overcurrent cut-off reliability.

3.3 Neo-6M GPS Module Performance

The geospatial benchmark demonstrates that the Neo-6M module can resolve latitude with an average relative error of 0.000575% and longitude with an average relative error of 0.000042%. In metric terms, the typical discrepancy from the reference GNSS is smaller than five meters, which is comparable to the specified horizontal accuracy of the module itself [33].

Table 6. Latitude Performance of the Neo-6M Module

No	GNSS Latitude	Neo-6M Latitude	Difference	Error (%)
1	-6.87026	-6.87023	0.003	0.000335%
2	-6.87032	-6.87030	0.002	0.000393%
3	-6.87080	-6.87082	0.002	0.000262%
4	-6.87088	-6.87083	0.005	0.000844%
5	-6.87089	-6.87092	0.003	0.000509%
6	-6.87086	-6.87084	0.002	0.000277%
7	-6.87089	-6.87084	0.005	0.000830%
8	-6.87029	-6.87023	0.006	0.000917%
9	-6.87007	-6.87004	0.003	0.000466%
10	-6.86992	-6.86977	0.015	0.002111%
11	-6.86949	-6.86945	0.004	0.000539%
12	-6.86916	-6.86914	0.002	0.000364%
13	-6.86919	-6.86912	0.007	0.001063%
14	-6.86949	-6.86942	0.007	0.001048%

Journal of Renewable Energy and Smart Device (JORESD)
E-ISSN : 3026-216X
P-ISSN : 3031-173X
Vol. 3, No. 2 April 2026
https://journal.globresco.com/index.php/JORESD

No	GNSS Latitude	Neo-6M Latitude	Difference	Error (%)
15	-6.86891	-6.86889	0.002	0.000247%
16	-6.86863	-6.86858	0.005	0.000684%
17	-6.86827	-6.86822	0.005	0.000801%
18	-6.86855	-6.86853	0.002	0.000248%
19	-6.86901	-6.86899	0.002	0.000306%
20	-6.86954	-6.86948	0.006	0.000815%
		Average		**0.000575%**

The longitude test results (average error 0.000042%) reflect the slightly smaller deviation on the east–west axis under the study location. This anisotropy is influenced by the geometry of the visible satellite constellation, which during the test session was favourable for the longitudinal component. To provide a more physically interpretable metric, the angular error values were converted to ground-distance equivalents using the standard approximation that one degree of latitude corresponds to approximately 111,139 meters at the Earth's surface. Applying this conversion to the average latitude error of 0.000575° yields an average positional discrepancy of approximately 0.639 meters, while the maximum single-point latitude error of 0.015° (data point 10) corresponds to approximately 1.67 meters. For longitude, one degree at latitude 6.87° corresponds to approximately 110,490 meters, so the average longitude error of 0.000042° translates to approximately 0.046 meters. These values confirm that the Neo-6M module achieves sub-2-meter accuracy under the open-sky campus conditions of this study, which is well within the 100-meter geofence radius configured as the system default.

The reported accuracy is adequate for mapping the e-bike to a street-level resolution on Google Maps and therefore supports the proposed geofencing functionality. These results are consistent with those reported by Moumen et al [34] who evaluated the Neo-6M GPS module in a real-time IoT vehicle tracking system and recorded sub 3 meter positional accuracy under open-sky conditions after applying Kalman filter post-processing. The accuracy obtained in this study, without additional filtering, falls within the range expected for unprocessed GNSS output and is sufficient for street-level geofencing and theft location reporting.

It is important to acknowledge that the accuracy figures reported above were obtained under open-sky campus conditions, where the Neo-6M module had an unobstructed view of the satellite constellation. In densely built urban environments which represent the primary deployment context for this system building facades, overpasses, and narrow street canyons introduce multipath propagation errors that can degrade positional accuracy to between 5 and 15 meters, as documented in comparable low-cost GNSS evaluations conducted in urban settings [33]. While this level of degradation remains well within the 100-meter geofence radius configured as the system default, it may reduce the precision of theft-location reporting in dense city areas. Future work should therefore include field validation of the Neo-6M module under representative urban riding conditions in Indonesian cities to characterise the actual positional uncertainty experienced by end users.

3.4 System Integration and Cut-off Validation

The factorial integration test investigated the system response to all eight combinations of normal and abnormal values across the three electrical parameters. In every abnormal scenario, the LCD, the buzzer, the Telegram bot, the website dashboard, and the cut-off relay were activated simultaneously, confirming the correctness of the Boolean OR logic. Only the all-normal scenario kept every output in an inactive state, as expected.

Table 7. Integration Test of the Multi Parameter Response

No	Voltage	Current	Temperature	LCD	Buzzer	Telegram	Website	Cut-off
1	Normal	Normal	Normal	x	x	x	x	x
2	High	Normal	Normal	✓	✓	✓	✓	✓
3	Normal	High	Normal	✓	✓	✓	✓	✓

Journal of Renewable Energy and Smart Device (JORESD)
E-ISSN : 3026-216X
P-ISSN : 3031-173X
Vol. 3, No. 2 April 2026
https://journal.globresco.com/index.php/JORESD

No	Voltage	Current	Temperature	LCD	Buzzer	Telegram	Website	Cut-off
4	Normal	Normal	High	✓	✓	✓	✓	✓
5	High	High	Normal	✓	✓	✓	✓	✓
6	High	Normal	High	✓	✓	✓	✓	✓
7	Normal	High	High	✓	✓	✓	✓	✓
8	High	High	High	✓	✓	✓	✓	✓

Based on Table 6 subsequent validation of the cut-off mechanism addressed six operational conditions, including three parameter-triggered faults and two remotely commanded actions. The relay-based cut-off architecture adopted in this study aligns with the multi-fault detection paradigm validated in prior IoT protection systems, where a single relay module controlled by a microcontroller was demonstrated to successfully isolate faults across overvoltage, overcurrent, and over-temperature conditions with sub-second response times every scenario [35], with the largest delay reaching one second under overtemperature, which originates from the one-second sampling window applied to the DS18B20. The obtained latency is well within the reaction time expected from multi-parameter thermal runaway warning systems reported in the literature [36], where the critical delay threshold before catastrophic failure typically exceeds several seconds.

Table 8. Performance of the Automatic Cut-off Mechanism

No	Condition	Relay	Delay (s)	Result	Status
1	Normal	ON	0	E-bike operates	Success
2	Overvoltage	OFF	2	E-bike stops	Success
3	Overcurrent	OFF	1	E-bike stops	Success
4	Overtemperature	OFF	1	E-bike stops	Success
5	Remote Lock	OFF	1	E-bike stops	Success
6	Remote Unlock	ON	1	E-bike operates	Success

Table 7 presents the automatic cut-off mechanism test across six conditions. Under normal parameters the relay remained ON with zero delay. Overvoltage produced the longest delay at 2 seconds, reflecting the additional time for HTTP POST and Telegram notification dispatch before cut-off confirmation. Overcurrent and overtemperature each recorded 1 second, consistent with the Modbus-RTU and OneWire sensor polling intervals respectively. Remote Lock and Unlock via Telegram also registered 1 second, attributable to the ESP32 polling the server command endpoint at one-second intervals. All six scenarios returned Success, confirming a 100% success rate. The maximum delay of 2 seconds remains well within the acceptable response window for battery protection applications where fault escalation develops from seconds to minutes.

Journal of Renewable Energy and Smart Device (JORESD)
E-ISSN : 3026-216X
P-ISSN : 3031-173X
Vol. 3, No. 2 April 2026
https://journal.globresco.com/index.php/JORESD

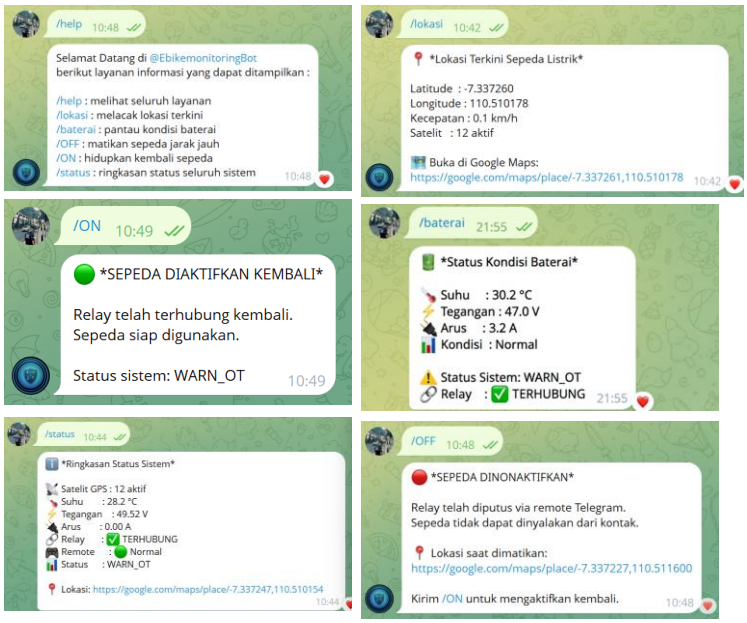

Figure.13. Button Functions on Telegram Bot

Figure 13 presents the actual output of each command function captured during system testing. The /help command returns a complete list of available commands with brief descriptions, confirming correct bot initialization. The /lokasi command delivers real-time GPS data including coordinates, speed, satellite count, and a Google Maps link, verifying successful NMEA data parsing from the Neo-6M module. The /baterai command returns a formatted panel showing temperature (30.2°C), voltage (47.0 V), current (3.2 A), battery condition, and relay state, confirming correct sensor data packaging from both the PZEM-017 and DS18B20. The /ON and /OFF commands each return relay state confirmation accompanied by system status and last-known GPS coordinates, demonstrating correct remote actuation via Telegram. The /status command consolidates all active parameters into a single diagnostic summary covering GPS, thermal, electrical, and relay data simultaneously. All six command outputs are consistent with the system design specifications, confirming that the Telegram Bot interface operates correctly as a real-time monitoring and remote-control channel for the electric bicycle system.

Table 9. Telegram Command Test

No	Response Time (s)	Voltage (V)		Temperature (°C)		Current (A)		Result
		Bot	Website	Bot	Website	Bot	Website	
1	1.8	52.4	52.4	33.1	33.1	2.14	2.14	Match
2	2	52.5	52.5	33.3	33.3	2.16	2.16	Match
3	1.7	52.3	52.3	33	33	2.13	2.13	Match
4	2.1	52.6	52.6	33.4	33.4	2.14	2.14	Match
5	1.9	52.4	52.4	33.2	33.2	2.15	2.15	Match
6	2.3	52.5	52.5	33.1	33.1	2.14	2.14	Match
7	1.8	52.3	52.3	33.3	33.3	2.13	2.13	Match
8	2	52.4	52.4	33.2	33.2	2.15	2.15	Match
9	1.9	52.6	52.6	33	33	2.14	2.14	Match
10	2.2	52.5	52.5	33.4	33.4	2.16	2.16	Match
Avg	1.97	52.45	52.45	33.20	33.20	2.14	2.14	100% Match

Journal of Renewable Energy and Smart Device (JORESD)
E-ISSN : 3026-216X
P-ISSN : 3031-173X
Vol. 3, No. 2 April 2026
https://journal.globresco.com/index.php/JORESD

Based on Table. 9 All 10 trials of the /battery command returned complete payloads with sensor values identical to those displayed on the web dashboard, confirming 100% data consistency between the Telegram Bot and the website output channel. Response times ranged from 1.7 to 2.3 seconds with a mean of 1.97 seconds, well within the 5 second threshold defined in the test protocol. The variation of 0.6 seconds across trials is attributable to non-deterministic factors including the Modbus-RTU and OneWire sensor polling intervals now each command was received, and variable queue processing time on the Telegram server. The small natural fluctuation in sensor readings across trials voltage between 52.3–52.6 V, temperature between 33.0–33.4°C, and current between 2.13–2.16 A reflects normal battery behavior under constant low-level discharge and remained entirely within the safe thresholds defined in Table 1 throughout all trials.

3.5 Website and Telegram Notification Latency

Notification latency was measured across five operating scenarios, ranging from the nominal condition to the four abnormal conditions corresponding to overvoltage, undervoltage, overcurrent, and overtemperature. The web dashboard received data every twenty seconds in normal operation and between one and three seconds when a critical event was triggered. The Telegram bot delivered alerts within zero to one second, in line with the responsive performance reported by Isyanto et al. who measured an average of 2.776 seconds for their IoT vehicle security system [17].

Table 10. IoT System Performance Metrics

No	Metric	Value	Basis
1	Data throughput normal mode	3 records/min	20-second polling interval programmed in ESP32 firmware
2	Data throughput fault mode	20–60 records/min	1–3 second interval triggered automatically upon threshold breach
3	Packet loss rate	0%	10 trials per scenario; all HTTP POST requests confirmed 200 OK response
4	Telegram delivery success rate	100%	10 trials per /battery command, all messages confirmed delivered
5	Dashboard Telegram data consistency	100%	Payload values identical across both output channels in all trials
6	Mean Telegram notification latency	1.97 s	Range 1.7–2.3 s across 5 fault scenarios (normal, Over Voltage, Under Voltage, Over Current, Over Temperature)
7	Maximum cut-off response delay	2 s	Overvoltage scenario; includes HTTP POST and Telegram dispatch time
8	System uptime during testing	100%	No microcontroller reset or watchdog timeout recorded across all sessions

Table 10 summarizes the IoT-layer performance metrics recorded during structured system testing. A packet loss rate of zero percent confirms that the HTTP communication channel between the ESP32 and the Laragon server maintained reliable connectivity throughout all test sessions, with every POST request receiving a confirmed 200 OK response. Data throughput scaled automatically from three records per minute under normal conditions to up to sixty records per minute during fault events, demonstrating proportional firmware response without manual intervention. The one-hundred-percent system uptime with no microcontroller reset or watchdog timeout recorded confirms that the ESP32-Laragon-Telegram stack is sufficiently stable for continuous unattended deployment on an electric bicycle.

Journal of Renewable Energy and Smart Device (JORESD)
E-ISSN : 3026-216X
P-ISSN : 3031-173X
Vol. 3, No. 2 April 2026
https://journal.globresco.com/index.php/JORESD

Table 11. Website and Telegram Notification Latency

No	Condition	Website Status	Website Delay (s)	Telegram Status	Telegram Delay (s)
1	Normal	Displayed	1	Inactive	0
2	Overtemperature	Displayed	2	Active	1
3	Overvoltage	Displayed	1	Active	1
4	Low voltage	Displayed	1	Active	0
5	Overcurrent	Displayed	3	Active	1

The Telegram notification latency of zero to one second recorded in this study is in line with findings from Abu Zaid et al. [37], who implemented a Telegram Bot-based IoT emergency alert system and measured consistent notification delivery within two seconds under normal Wi-Fi conditions. The slight variation in delay observed across different fault scenarios in this study can be attributed to differences in Wi-Fi signal stability and the Telegram server polling interval, both of which introduce non-deterministic jitters that are acceptable for battery protection applications where the fault evolution timescale is measured in seconds to minutes, not milliseconds.

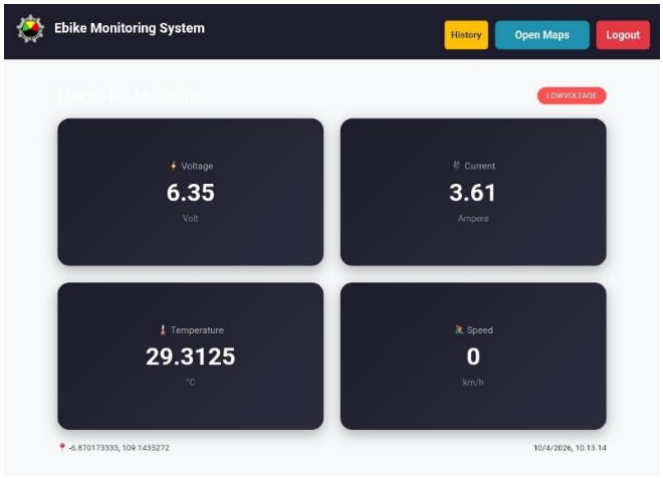

Figure.14. Website Dashboard View

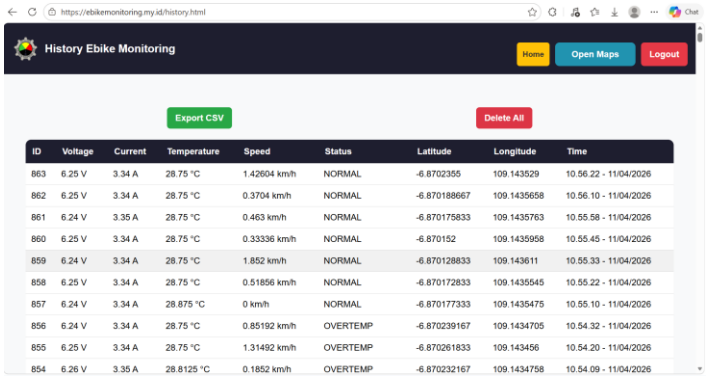

Figure.15. Data History View on the Website

Journal of Renewable Energy and Smart Device (JORESD)
E-ISSN : 3026-216X
P-ISSN : 3031-173X
Vol. 3, No. 2 April 2026
https://journal.globresco.com/index.php/JORESD

Figure 15 displays the real-time dashboard presenting four sensor parameter cards covering voltage, current, temperature, and vehicle speed, a system status indicator, current GPS coordinates, session timestamp, and header navigation buttons for accessing the history page, Google Maps view, and logout function.

Figure 16 presents the data history page displaying all sensor records stored in the MySQL database in tabular form with columns for voltage, current, temperature, speed, system status, latitude, longitude, and timestamp. Records are logged automatically every 20 seconds, and each entry carries a status label for fault traceability. An Export CSV button enables offline data analysis, and a Delete All option supports database maintenance.

3.6 Black Box Functional Validation

A Black-Box test was performed on the website application to ensure that functional requirements had been met. Nine scripted user interactions were executed, covering login, invalid authentication, sensor-driven alarms, GPS visualization, periodic data refresh, and Wi-Fi recovery. Every scenario yielded the expected outcome, confirming the correct binding between the back-end services and the front-end components [38].

Table 12. Black Box Testing

No	Test Activity	Expected Result	Test Result	Conclusion
1	User opens login page	Login form with username and password fields is displayed	Login page displayed correctly	Success
2	Login with valid credentials	System validates data and redirects to dashboard	User reaches the dashboard	Success
3	Login with invalid credentials	System rejects access and shows error message	Error message appears	Success
4	Sensor detects overvoltage	LCD warning, buzzer, Telegram alert, relay cut-off	Full response observed	Success
5	Sensor detects overcurrent	LCD warning, buzzer, Telegram alert, relay cut-off	Full response observed	Success
6	Sensor detects overtemperature	LCD warning, buzzer, Telegram alert, relay cut-off	Full response observed	Success
7	GPS module sends coordinates	Lat–long shown on website with Google Maps link via Telegram	Data displayed; Maps link functional	Success
8	Sensor data sent every 20 s	Website updates history table periodically	Periodic update confirmed	Success
9	Wi-Fi disconnects	System reconnects; LCD shows SSID status	Reconnection successful	Success

3.7 Comparison with Related IoT Battery Monitoring Studies

Table 13. Quantitative Benchmarking of the Proposed System Against Related IoT-Based Battery Monitoring Systems

No	Comparison Aspect	Ramadhan et al. [15] (2023)	Salsabila et al. [16] (2023)	Hutagaol et al. [31] (2022)	Andri et al. [5] (2023)	This Study (Proposed) (2025)
SYSTEM NOVELTY & KEY FEATURES						
1	Temperature monitoring	✓	X	X	✓	✓
2	GPS / location tracking	X	✓	X	X	✓
3	Automatic relay cut-off	X	X	X	✓	✓
4	Remote cut-off via application	X	X	X	X	✓

Journal of Renewable Energy and Smart Device (JORESD)
E-ISSN : 3026-216X
P-ISSN : 3031-173X
Vol. 3, No. 2 April 2026
https://journal.globresco.com/index.php/JORESD

No	Comparison Aspect	Ramadhan et al. [15] (2023)	Salsabila et al. [16] (2023)	Hutagaol et al. [31] (2022)	Andri et al. [5] (2023)	This Study (Proposed) (2025)
5	Anti-theft geofencing	X	X	X	X	✓
6	Dual-channel notification (Web + Telegram)	X	X	X	✓	✓
SENSOR PERFORMANCE (QUANTITATIVE)						
7	Voltage accuracy (%)	N/R	N/R	97.80%	N/R	98.78%
8	Current accuracy (%)	N/R	N/R	N/R	N/R	98.21%
9	Temperature accuracy (%)	N/R	N/R	N/R	N/R	98.87%
10	GPS positional error (avg.)	N/R	N/R	N/R	N/R	< 2 m
11	Inferential statistical validation (paired t-test, n = 20 per sensor)	X	X	X	X	✓
COMMUNICATION & IoT METRICS (QUANTITATIVE)						
12	Notification channel	Blynk	Web	Web	Telegram	Web + Telegram
13	Mean notification latency	N/R	N/R	N/R	N/R	1.97 s (σ = 0.12 s)

**Notes*
✓ = Feature present
X = Feature absent
N/R = Not Reported by the respective study

Table 13 benchmarks the proposed system against four related studies across three dimensions. In terms of system novelty, this study is the only one to simultaneously integrate automatic relay cut-off, remote cut-off, anti-theft geofencing, and dual-channel notification. Regarding sensor performance, this study reports the highest voltage accuracy (98.78%) among comparable works, while current, temperature, and GPS error metrics remain unreported in all compared studies. This study is also the only one to apply paired t-test validation across n = 20 calibration points per sensor and achieved a mean notification latency of 1.97 seconds a metric absent from all compared works. These results confirm that the proposed system advances the state of the art by unifying multi-parameter protection, active fault isolation, and statistically validated performance within a single low-cost platform.

3.8 System Power Consumption and Battery Endurance

An additional consideration for practical deployment is the power consumption of monitoring electronics relative to the host battery capacity. The ESP32 DevKit V1 draws approximately 240mA during active Wi-Fi transmission and 80mA in modem-sleep mode [measured from datasheet]. The PZEM-017 consumes approximately 1.5W from the RS-485 supply. The DS18B20 draws 1mA during conversion. Combined, the monitoring subsystem consumes an estimated peak of 2.7W during active transmission cycles, which represents approximately 0.28% of the 48V × 20.2Ah = 969.6Wh energy capacity of the host battery. This parasitic load is negligible for normal operating sessions and does not meaningfully affect the reported range of the electric bicycle. However, for extended stationary monitoring, the continuous draw over 8 hours would consume approximately 21.6Wh, equivalent to 2.2% of total capacity and acceptable overhead for the safety benefit provided.

Journal of Renewable Energy and Smart Device (JORESD)
E-ISSN : 3026-216X
P-ISSN : 3031-173X
Vol. 3, No. 2 April 2026
https://journal.globresco.com/index.php/JORESD

4. CONCLUSION

An integrated monitoring and security system for electric bicycles has been successfully designed, prototyped, and empirically validated. The combination of the PZEM-017, DS18B20, and Neo-6M modules orchestrated by an ESP32 microcontroller enables simultaneous observation of voltage, current, temperature, and geospatial position in real time. The empirical study confirmed high-fidelity measurement at every stage of the signal path, with the DS18B20 achieving an average accuracy of 98.867%, the PZEM-017 reaching 98.776% and 98.213% for voltage and current respectively, and the Neo-6M delivering a positional error below 0.001% on both axes. The automatic cut-off mechanism operated correctly in all six tested scenarios, and the Telegram notification pipeline propagated alerts within an average of two seconds after the onset of an abnormal event.

This study is the first to integrate automatic relay cut-off, dual-channel notification, and anti-theft geofencing within a single ESP32-based platform with inferential statistical validation, distinguishing it from prior works that address monitoring or security in isolation. The proposed system demonstrates real-world deployment potential as a low-cost safety module for the growing electric bicycle market in Indonesia, where standardised onboard battery protection for low-speed electric bicycles remains absent. Despite the encouraging results, several limitations must be acknowledged. The system's connectivity depends entirely on a stable Wi-Fi network; field conditions outside covered areas would interrupt real-time data transmission and Telegram notifications. The prototype was evaluated under laboratory-controlled fault conditions using regulated power supplies and controlled heat sources validation under actual road-riding conditions with vibration, variable ambience temperature, and dynamic load cycles remain a subject for future study. Additionally, only a single prototype unit was fabricated and tested, so manufacturing variability in sensor behaviour has not yet been characterised.

Future research will extend this work in four directions. First, a more sophisticated battery management algorithm incorporating state-of-charge estimation and cell balancing will be integrated to enable predictive fault detection rather than purely reactive threshold-based protection. Second, a GSM/4G cellular fallback channel will be implemented to preserve Telegram notification and remote cut-off capability in locations outside Wi-Fi coverage, addressing the primary connectivity limitation identified in this prototype. Third, the system will be evaluated in a longitudinal field study over at least 90 days of actual urban riding conditions, including exposure to road vibration, rain, and dynamic load cycles, to characterize hardware reliability under realistic operational stresses. Fourth, the scalability of the proposed architecture will be explored toward integration with broader e-mobility platforms, including electric motorcycles and three-wheeled cargo e-vehicles commonly used in Indonesian last-mile logistics, as the sensor selection and firmware architecture are agnostic to battery chemistry and can be adapted with minimal reconfiguration.

REFERENCES

[1] I. K. Wei Chen, Majed Alharthi, Jinjun Zhang, “The need for energy efficiency and economic prosperity in a sustainable environment,” *Gondwana Res.*, vol. Volume 127, 2024, [Online]. Available: https://doi.org/10.1016/j.gr.2023.03.025.%0A

[2] S. N. Aqmarina, R. Nurcahyo, and S. Sumaedi, “Accelerating Electric Motorcycle Adoption : Comparison Between Users and Non-Users Perspectives In Jakarta , Indonesia,” vol. 13, no. 2, pp. 1633–1644, 2024, doi: 10.18421/TEM132.

[3] J. R. Woo, H. Choi, and J. Ahn, “Well-to-wheel analysis of greenhouse gas emissions for electric vehicles based on electricity generation mix: A global perspective,” *Transp. Res. Part D Transp. Environ.*, vol. 51, pp. 340–350, Mar. 2017, doi: 10.1016/J.TRD.2017.01.005.

[4] I. E. Agency, “World Energy Outlook,” 2024.

[5] D. A. Andri, A. A. Ahfas, and I. S. Indah, “Sistem Monitoring Dan Protection Smart Charger Baterai Mobil Listrik Lithium Ion Berbasis Telegram,” *JEECOM J. Electr. Eng. Comput.*, vol. 5, no. 2, pp. 200–207, 2023, doi: 10.33650/jeecom.v5i2.6876.

[6] T. M. Bandhauer, S. Garimella, and T. F. Fuller, "A Critical Review of Thermal Issues in Lithium-Ion Batteries," *J. Electrochem. Soc.*, vol. 158, no. 3, p. R1, 2011, doi: 10.1149/1.3515880.
[7] X. Gu *et al.*, "Early warning of thermal runaway based on state of safety for lithium-ion batteries," pp. 1–9, 2025, doi: 10.1038/s44172-025-00442-1.
[8] D. Han, J. Wang, C. Yin, and Y. Zhao, "Advances in Early Warning of Thermal Runaway in Lithium-Ion Battery Energy Storage Systems," vol. 2400165, pp. 1–21, 2025, doi: 10.1002/adsr.202400165.
[9] R. Bromo, "Sepeda Listrik Meledak saat Dicas, Rumah Warga Dringu Probolinggo Terbakar." [Online]. Available: https://radarbromo.jawapos.com/probolinggo/1005296961/sepeda-listrik-meledak-saat-dicas-rumah-warga-dringu-probolinggo-terbakar
[10] CNN Indonesia, "Sepeda Listrik Meledak di Sulsel, Nenek dan 2 Anak Tewas Terbakar." [Online]. Available: https://www.cnnindonesia.com/nasional/20251126084411-20-1299490/sepeda-listrik-meledak-di-sulsel-nenek-dan-2-anak-tewas-terbakar
[11] D. Shi *et al.*, "A review of the combined effects of environmental and operational factors on lithium-ion battery performance: temperature, vibration, and charging/discharging cycles," *RSC Adv.*, vol. 15, no. 17, pp. 13272–13283, 2025, doi: 10.1039/d5ra00934k.
[12] S. D. Putri, Y. Sugiarti, and A. Fithry, "Legalitas Penggunaan Sepeda Listrik Di Tinjau Dari Perspektif UU No 22 Tahun 2009 Tentang Lalu Lintas Dan Angkutan Jalan," *J. Ilm. Wahana Pendidik.*, vol. 10, no. 1, pp. 773–785, 2024.
[13] X. Ma, J. Li, Z. Guo, and Z. Wan, "Role of big data and technological advancements in monitoring and development of smart cities," *Heliyon*, vol. Volume 10, no. Issue 15, 2024.
[14] T. N. V Krishna, S. V. S. V Prabhu, D. Kumar, S. S. Rao, and L. Chang, "Powering the Future : Advanced Battery Management Systems (BMS) for Electric Vehicles," *Energies*, 2024, doi: https://doi.org/10.3390/en17143360.
[15] A. W. Ramadhan, I. Permatasari, and A. T. Hidayat, "Monitoring Kinerja Baterai Skuter Listrik Berbasis IOT," *J. Electron. Electr. Power Appl.*, vol. 3, no. 2, pp. 181–188, 2023.
[16] T. T. Salsabila, H. F. Ramadhan, I. Imawati, and D. A. R. Wati, "EM-IOT: IoT-Based Battery Monitoring System and Location Tracking on Electric Vehicles," *Bul. Ilm. Sarj. Tek. Elektro*, vol. 5, no. 2, pp. 218–229, 2023, doi: 10.12928/biste.v5i2.8053.
[17] H. Isyanto, H. Muchtar, and A. R. Dinata, "Design of Security System Device for Motorized Vehicles through the Telegram Messenger Application and Updating GPS Locations on Smartphones in Real Time with IoT-based Smart Vehicles," vol. 6, no. 2, pp. 67–76, 2022.
[18] G. V. Lohar and M. S. Kumar, "Design and Implementation of IoT Based Wireless Battery Management System for Electric Vehicles," *Int. J. Intell. Syst. Appl. Eng.*, vol. 11, no. 10s, pp. 360–369, 2023.
[19] R. I. Putri, D. Radianto, and Z. Amalia, "Development of a Real-Time Monitoring Model for Solar-Powered Street Lighting Systems Using Internet of Things," vol. 15, no. 6, pp. 29186–29193, 2025.
[20] Sugiyono, *Metodologi Penelitian Kuantitatif, Kualitatif dan R & D*. Bandung: Alfabeta, 2020.
[21] A. Y. Chandra and W. Setyaningsih, "Benchmarking Local Development Environments: Analyzing the Performance of XAMPP, MAMP, and Laragon," *Bull. Comput. Sci. Res.*, vol. 5, no. 3, pp. 193–206, 2025, doi: 10.47065/bulletincsr.v5i3.493.
[22] D. Hercog, T. Lerher, and M. Truntič, "Design and Implementation of ESP32-Based IoT Devices," vol. 23, no. 1, 2023, doi: https://doi.org/10.3390/s23156739.
[23] MathWorks, "'ThingSpeak Licensing FAQ,' ThingSpeak IoT Platform," 2024, [Online]. Available: https://thingspeak.mathworks.com/pages/license_faq
[24] R. Delfianti, V. A. Tazayul, B. Mustaqim, F. Nusyura, and C. Harsito, "Internet of Things (IoT) based Electrical Power Monitoring System for Solar Power Plants using the Telegram Application," vol. 2, no. 3, pp. 428–443, 2025, doi: 10.26740/vubeta.v2i3.39405.
[25] M. I. El-afifi, B. E. Sedhom, S. Padmanaban, and A. A. Eladl, "A review of IoT-enabled smart energy hub systems : Rising , applications , challenges , and future prospects," *Renew. Energy Focus*, vol. 51, no. August, p. 100634, 2024, doi: 10.1016/j.ref.2024.100634.
[26] L. Li, Z. Li, J. Zhao, and W. Guo, "Lithium-Ion Battery Management System for Electric Vehicles Lithium-

Ion Battery Management System for Electric Vehicles," no. December 2018, 2022, doi: 10.23940/ijpe.18.12.p28.31843194.

[27] Battery University, "Charging Lead Acid," Battery University. [Online]. Available: https://www.batteryuniversity.com/article/bu-403-charging-lead-acid/

[28] Y. N. Hilal, "ANALISA BALANCING BMS (BATTERY MANAGEMENT SYSTEM) PADA PENGISIAN BATERAI LITHIUM-ION TIPE INR 18650 DENGAN METODE CUT OFF," vol. 14, no. 2, pp. 367–373, 2023.

[29] U. AG, "NEO-6 u-blox 6 GPS Modules Data Sheet," Thalwil, Switzerland, 2011. [Online]. Available: https://content.u-blox.com/sites/default/files/products/documents/NEO-6_DataSheet_(GPS.G6-HW-09005).pdf

[30] J. V. Hutagaol, D. Setiawan, and H. Eteruddin, "Perancangan Sistem Monitoring Kendaraan Listrik," *J. Tek.*, vol. 16, no. April, pp. 96–102, 2022.

[31] M. B. R. Huda and W. D. Kurniawan, "Analisa Sistem Pengendalian Temperatur Menggunakan Sensor DS18B20 Berbasis Mikrokontroler Arduino," *J. Rekayasa Mesin*, vol. 7, no. 2, pp. 18–23, 2022.

[32] F. H. Gandoman, E. M. Ahmed, Z. M. Ali, M. Berecibar, A. F. Zobaa, and S. H. E. Abdel Aleem, "Reliability evaluation of lithium-ion batteries for e-mobility applications from practical and technical perspectives: A case study," *Sustain.*, vol. 13, no. 21, 2021, doi: 10.3390/su132111688.

[33] J. Andreas and M. Fathurahman, "Analisis Tingkat Akurasi NEO-6M dengan Google Maps," *Semin. Nas. Inov. VOKASI*, vol. 4, no. 1, pp. 1018–1023, 2025.

[34] I. Moumen, N. Rafalia, and J. Abouchabaka, "Real - time GPS Tracking System for IoT - Enabled Connected Vehicles," vol. 01095, 2023.

[35] S. Neharkar, Bhimrao & Patil, Shubham & Sarkar, Sushmita & Tekam, "IoT-based overvoltage, overcurrent, and over-temperature fault detector in industries," *J. IoT Smart Autom.*, vol. 1, pp. 1–6, 2023.

[36] W. L. Jianfeng Wang, Bowei Chen, Yuhan Li, Ting Hu, Fen Liu, Mengyu Shi, Xutong Ren, Yongkai Jia, "Multiparameter warning of lithium-ion battery overcharge-thermal runaway," *J. Energy Storage,* vol. VOlume 78, 2024, [Online]. Available: https://doi.org/10.1016/j.est.2023.110088.

[37] N. N. S. Abu.Zaid, Muhammad and Abdullah, Rina and Izawana, Syila and Nik Dzulkefli, "IoT-based Emergency Alert System Integrated with Telegram Bot," *IEEE Int. Conf. Autom. Control Intell. Syst.*, pp. 126–131, 2023.

[38] M. Mintarsih, "Pengujian Black Box Dengan Teknik Transition Pada Sistem Informasi Perpustakaan Berbasis Web Dengan Metode Waterfall Pada SMC Foundation," *J. Teknol. Dan Sist. Inf. Bisnis*, vol. 5, no. 1, pp. 33–35, 2023, doi: 10.47233/jteksis.v5i1.727.